Journal of Power Sources 258 (2014) 61–75

Contents lists available at ScienceDirect

Journal of Power Sources

journal homepage: www.elsevier.com/locate/jpowsour

Electrochemical characterization and post-mortem analysis of aged $LiMn_2O_4$–NMC/graphite lithium ion batteries part II: Calendar aging

Barbara Stiaszny [a], Jörg C. Ziegler [a,*], Elke E. Krauß [a], Mengjia Zhang [a], Jan P. Schmidt [b], Ellen Ivers-Tiffée [b]

[a] Robert Bosch GmbH, Corporate Sector Research and Advance Engineering, Postfach 10 60 50, 70049 Stuttgart, Germany
[b] Institut für Werkstoffe der Elektrotechnik (IWE), Karlsruher Institut für Technologie (KIT), Adenauerringer 20b, 76131 Karlsruhe, Germany

HIGHLIGHTS

- Comprehensive analysis of new and calendar aged cells by numerous methods.
- Application of the DRT to impedance spectra.
- Aged anodes show a reduced overall impedance.
- Dominant aging mechanisms have been clarified.

ARTICLE INFO

Article history:
Received 18 November 2013
Received in revised form
14 January 2014
Accepted 6 February 2014
Available online 15 February 2014

Keywords:
Aging mechanisms
Calendar aging
$LiMn_2O_4$
NMC
Lithium ion battery
EIS

ABSTRACT

A detailed post-mortem analysis was carried out for commercial lithium ion batteries stored at 4.2 V and 4.0 V at 60 °C. Complementary electrochemical and physical–analytical investigations revealed that the most significant aging processes for the cells aged at 4.2 V were loss of cycleable lithium, decomposition of the electrolyte and loss of active cathode material ($LiMn_2O_4$/$Li(Ni_{0.5}Mn_{0.3}Co_{0.2})O_2$). The cells aged at 4.0 V also exhibited loss of cycleable lithium, but at a smaller extent. In fact, the aged anodes did not show significant changes compared to the new anode.

Electrochemical impedance measurements including symmetric laboratory test cells gained from new and aged cells revealed valuable information about changing charge-transfer processes. The 4.2 V-cathode and both aged anodes surprisingly exhibited a decreased charge-transfer resistance, while the 4.0 V-cathode's charge-transfer resistance increased.

1. Introduction

High power and energy density of lithium ion batteries made them one of the most attractive energy storage systems. Nowadays they are widely used in portable electronic devices like laptops, cameras and mobile phones. In the past few years lithium ion batteries have drawn much attention for their operation in automotive applications like hybrid vehicles (HEV), plug-in hybrid electric vehicles (PHEV) and full electric vehicles (EV). These applications require long cycle and calendar life, typically up to 15 years, low cost, high power and safe operation.

Although there is a large variety of possible materials combinations for electrodes in lithium ion batteries, combining high cycle stability and high specific capacity reduces the choices to only a few. Promising candidates for cathodes are layered oxides like $Li(Ni_{1/3}Co_{1/3}Mn_{1/3})O_2$ which exhibits high specific capacity [1], but discharge at high rates is limited. Improving safety and especially rate capability of the cell, $LiMn_2O_4$ is added to the cathode because it exhibits the fast kinetics necessary for high power applications [1]. Mn-rich compounds are preferred compared to Ni- or Co-rich materials since they reduce the battery's cost, although their specific capacity is lower and $LiMn_2O_4$ suffers from rapid degradation especially at elevated temperatures due to manganese dissolution [1,2]. The best anode material considering both specific capacity and cycleability is graphite [2].

It is commonly known that the lifetime of lithium ion batteries is limited by unwanted side reactions [3]. These side reactions may affect all parts of a battery including the electrolyte, the active materials, binder, conducting agents, current collectors and the

* Corresponding author. Tel.: +49 711 811 7626; fax: +49 711 811 5119333.
E-mail address: joerg.ziegler@de.bosch.com (J.C. Ziegler).

http://dx.doi.org/10.1016/j.jpowsour.2014.02.019
0378-7753/

separator, resulting in capacity decrease and/or increase of the overall cell impedance [3–5]. Especially the electrolyte's components are sensitive to exposure at elevated temperatures.

Calendar aging arises independently from other stress like cycling and is permanently present. In daily use lithium ion batteries are often exposed to great stress like high ambient temperature and high storage voltages. This may influence electrochemical processes, kinetics and safety of the cells. Understanding the relevant aging mechanisms in lithium ion batteries is of great importance to face lifetime and safety challenges and to make precise lifetime predictions.

In this work aging phenomena arising from calendar aging are investigated by several physical–analytical methods as well as electrochemical impedance spectroscopy.

2. Experimental

2.1. Cell type

Commercial 18650 lithium ion batteries containing a blend of $LiMn_2O_4$ and $Li(Ni_{0.5}Mn_{0.3}Co_{0.2})O_2$ as cathode material and graphite as anode material with an initial capacity of 2 Ah have been used in this work.

2.2. Cell storage

Prior to calendar aging the cells were characterized by a power and capacity test. In order to determine the power and inner resistance 12 A discharge pulses were applied for 10 s at different SOCs (between SOC100 and SOC10 in steps of 10% SOC). The voltage and current were taken just prior to the pulse and at the end of the pulse after 10 s to calculate the inner resistance by the following Equation (1).

$$R_{DC} = \frac{U_{10s} - U_{0s}}{I_{10s} - I_{0s}} = \frac{\Delta U}{\Delta I} \quad (1)$$

The specific power in W kg^{-1} was calculated by multiplication of voltage and current at the end of the pulse after 10 s divided by the mass of the cell as shown in Equation (2).

$$P = \frac{U_{10s} \cdot I_{10s}}{m_{Cell}} \quad (2)$$

The capacity was determined at a discharge rate of 1C and C/5. The cells were discharged to a voltage of 2.75 V as recommended by the cell supplier.

After the power and capacity test, the standard charging procedure recommended by the manufacturer was applied. Cells were charged at a constant current rate of 2 A from 2.75 V to 4.2 V and subsequently the voltage was held constantly at 4.2 V until the total charging time exceeded 3 h.

Eight identical cells are stored at 60 °C, five cells at a voltage of 4.2 V (SOC100) and three at 4.0 V. The batteries are stored at open circuit potential, thus no trickle charge is applied and the cell is allowed to change its voltage by self-discharge between two characterization segments. During storage specific power, 1C and C/5 capacity are monitored every 20 days. The characterization was carried out with a Battery Cycler (BaSyTec GmbH, Germany) at room temperature.

2.3. Laboratory test cells

For post-mortem analysis and further inspection of the new and aged cells, the batteries were opened in an argon-filled glovebox. Electrode disks with a diameter of 18 mm were punched out for use in laboratory test cells (EL-Cells, EL-Cell GmbH, Germany) [6]. Before using the electrode sheets the coating had to be removed on one side of the current collector in order to get electrical contact in the EL-Cells. Particularly with aged electrodes the coating easily flakes off or sticks to the separator, making it a challenge to gain fully coated electrode sheets. After removing the coating the sheet was washed in dimethyl carbonate to remove any residuals from the electrolyte and dried afterward at room temperature. The preparation procedure, together with the fact that the coating of the aged electrodes easily flakes off makes it nearly impossible to investigate surface layers or contact resistances between the active material and the current collector.

For all laboratory test cells a glass fiber separator (EL-Cell GmbH, Germany) with a diameter of 18 mm and a thickness of 1.55 mm served as the electrolyte reservoir. 1 M $LiPF_6$ in a mixture of ethylene carbonate (EC) and dimethyl carbonate (DMC) at a ratio of 1:1 (v/v%) was used as the electrolyte in the laboratory test cells.

In total three types of laboratory test cells were prepared.

- *Half cells* having anode or cathode as working electrode and metallic lithium as counter and reference electrode (e.g. data shown in Fig. 10).
- *Full cells* with cathode and anode plus metallic lithium as reference electrode to monitor the potentials of anode and cathode during cycling (e.g. data shown in Figs. 11 and 12)
- *Symmetric cells* with two cathodes or two anodes [7], set to the same potential (e.g. data shown in Figs. 16 and 17)

2.4. Electrochemical investigation

A slow constant current discharge at C/50 was conducted at the aged electrode to distinguish between capacity fade from loss of active material and from increase of the inner resistance.

Slow-scan cyclic voltammetry was carried out at anode and cathode half cells at a scanning rate of 5 μV s^{-1} to investigate the redox voltages and peak heights of new and aged electrodes.

Furthermore half cells were subjected to rate tests with C-rates at C/10 and 1C to check the rate capability of new and aged electrodes.

Full cells with reference electrodes were assembled to measure the potentials of the anode and cathode during cycling of new and aged cells. In these experiments the potentials of anode and cathode were monitored against the Li-reference electrode while cycling the cell between 4.2 V and 2.75 V.

Electrochemical impedance spectroscopy (EIS) was carried out using a Gamry Instruments Potentiostat PCI4G300-51021 (Series-G300). Full batteries were discharged to SOC10 at a rate of C/5 and kept at OCV for four hours before the measurement started. The impedance of batteries was measured in pseudo-potentiostatic mode every 20 days during calendar aging in the frequency range between 10^5 Hz and 2 mHz with a perturbation voltage of 1 mV at temperatures of 23 °C, 0 °C and −10 °C. Laboratory test cells were directly investigated with EIS after assembly in a frequency range between $3{\cdot}10^5$ Hz and 2 mHz at the same perturbation voltage and at temperatures of 23 °C, 10 °C and 0 °C. Before the measurement the battery was kept for three hours at the desired temperature to be equilibrated. Temperature control was achieved in a climate chamber.

For the analysis and interpretation of the impedance spectra the DRT (distribution of relaxation times) method was applied. This method was introduced more than 10 years ago for the evaluation of impedance spectra measured from solid oxide fuel cells and is presented in-depth in Refs. [8–10]. As shown recently [11,12] it is also suitable to derive adequate equivalent circuit models for lithium-ion batteries.

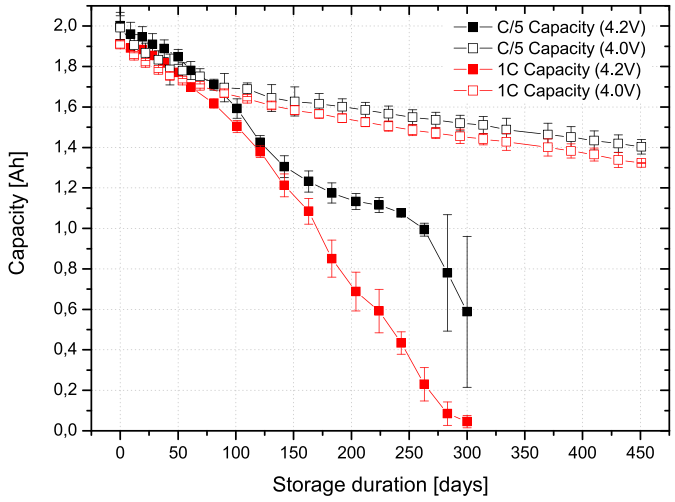

Fig. 1. Capacity decrease at 1C and C/5 discharge rate during calendar aging at 4.2 V and 4.0 V and 60 °C. Error bars representing standard deviation of five (4.2 V) or three (4.0 V) identical cells.

2.5. Physical–analytical investigation

Electrode sheets were washed in dimethyl carbonate and dried at room temperature in the glovebox before each investigation. XRD measurements were conducted with a Bruker D8 Advance with a wavelength of CuKα_1 = 1.5405 Å covering the diffraction-angle range $5 < \Theta < 85$. Before the XRD analysis the electrodes are set to SOC 0 corresponding to 835 mV vs. Li/Li$^+$ for the anode and 3.58 V vs. Li/Li$^+$ for the cathode. Surface investigations were done by a Gemini Leo 1530 scanning electron microscope equipped with Oxford Instruments analytical tools. For surface pictures typically an acceleration voltage of 5 kV was used, whereas for EDS analysis 20 kV was selected. Microsections investigated with a Zeiss Axioplan light microscope were used to determine layer thicknesses.

Concentrations of transition metals at the anode were ascertained by ICP-OES measurements, where the active material was removed from the current collector and was dissolved in nitro-hydrochloric acid.

As a reference state, a pristine cell was fully characterized by the designated methods, which is labeled as a “new cell” in the following text and graphs.

3. Results and discussion

3.1. Investigation of the new cell

The results of the investigation of the new cell were already described in our previous paper [13]. We fully characterized new cells using slow-rate electrochemical analysis, cyclic voltammetry, rate capability tests and electrochemical impedance spectroscopy as well as numerous analytical tools like ICP-OES, XRD, SEM/EDX and light microscopy.

3.2. Investigation of calendar aged cells stored at 4.2 V and 4.0 V

During storage the capacity was monitored at a discharge rate of 1C and C/5 as shown in Fig. 1. It can be seen that the capacity decreases drastically within 300 days for the 4.2 V-cell, while a reduction of 200 mV in storage voltage already reduces the capacity fade significantly. The C/5 and 1C curve for the cell stored at 4.2 V are moving apart at storage durations >180 days. This can be interpreted by a more significant increase of the inner resistance at storage durations >180 days (see Fig. 2b), which causes the continuous steep drop in Fig. 1, compared to the flattened C/5 curve. At the end of the black curve with the filled symbols quite high standard deviations of the cells can be seen. This is a result of differently pronounced capacity drops between the various cells especially at the end of their lifetime. 1C and C/5 curves of the 4.0 V-cell run at a comparable level, which is reflected by the power and inner resistance curves in Fig. 3a and b.

Furthermore the devolution of power and inner resistance at 10 different SOCs (SOC100 − SOC10) are plotted in Figs. 2 and 3. It is obviously that the power decreases with increasing storage duration. This is due to a continuous increase of the inner resistance of the cells.

Obviously the 4.2 V-cell suffers from prominent increase of the inner resistance after 300 days, which is about seven times higher compared to the new cell, while the inner resistance of the 4.0 V-cell increases about 1.5 times within 300 days and two times within 451 days. Conspicuously the curves in Fig. 2a converge at higher storage durations. The power of the cell at advanced storage durations keenly declined. Just after beginning of the 10 s pulse, the default current of 12 A is reduced, because the pulse reaches the lower voltage limit. This limits the power, which can be seen for all SOCs except SOC100, where the pulse can be fully performed with a current of 12 A, since the voltage does not reach the lower voltage limit. The 4.0 V-cell does not show this phenomenon, at each SOC

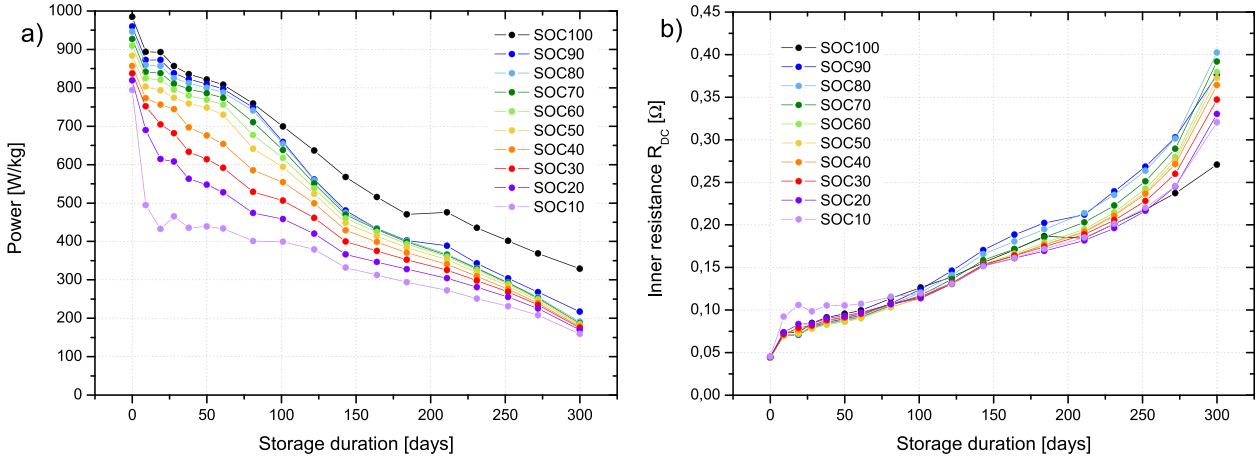

Fig. 2. Evolution of a) power and b) inner resistance for different SOCs during storage at 4.2 V and 60 °C.

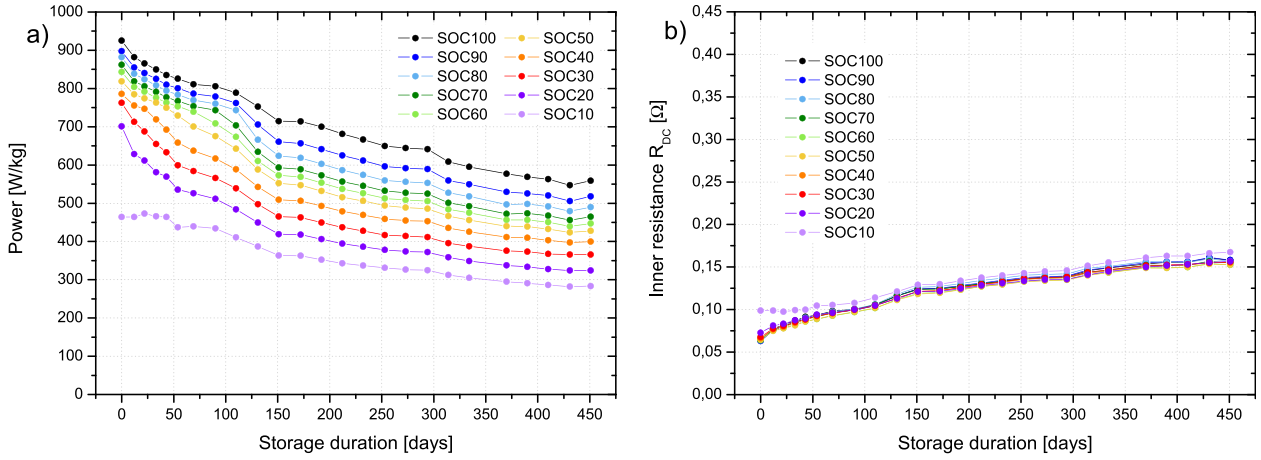

Fig. 3. Evolution of a) power and b) inner resistance for different SOCs during storage at 4.0 V and 60 °C.

the whole pulse can be conducted at 12 A without reaching the lower voltage limit.

3.3. Investigation of calendar aged cells stored at 4.2 V and 4.0 V by impedance spectroscopy

Figs. 4 and 5 depict the changing electrochemical impedance spectra during aging. The total impedance of the 4.2 V-cell after 300 days at 60 °C is twice as high as that of the 4.0 V-cell after 300 days at 60 °C. The shape of the spectra for the cell aged at 4.0 V and 60 C only varies slightly, while the cell aged at 4.2 V and 60 °C show large differences between the single spectra. This is due to a significant change of the OCV of the cells aged at 4.2 V. The 18650 cells are always set to SOC10. With increasing storage duration the open circuit voltage at SOC10 changes as shown in Fig. 6.

The reason for that is a changed cathode potential in the aged state (see later Figs. 11 and 12), which is due to loss of cycleable lithium. Lithium ions are captured in the solid electrolyte interface and are not available to fully discharge the cathode leading to a higher cathode potential. As already described in our previous paper [13], the charge-transfer process of the cathode is very sensitive to potential changes and impedance spectra of aged cells can give a mixture of aging- and potential-dependant influences, which are discussed in detail in Chapter 3.6.

One of the most prominent trends in the impedance spectra of both cells is the increase of the ohmic resistance which is ascribed mainly to the electrolyte resistance. At elevated temperatures the oxidizing properties of the cathode against the electrolyte is one of the most prominent aging factors [5]. Because the interface voltage (between cathode and electrolyte) is influenced by the state of charge more oxidization is expected in the 4.2 V case. Additionally the conductive salt in the electrolyte, namely $LiPF_6$, is not stable at elevated temperatures and decomposes as shown in the following Equation (3) [14]. The decomposition of the organic solvents and the conductive salt causes changes in the electrolyte's composition leading to a changed resistance of the electrolyte.

$$LiPF_6 \leftrightarrow LiF + PF_5 \quad (3)$$

To evaluate the extent of the changes the impedance spectra are fitted by an electrical equivalent circuit. In order to derive the correct equivalent circuit the DRT [11] was calculated from the impedance spectra to separate the occurring processes in the cell (see Fig. 7).

In Figs. 4 and 5 two semicircles can be observed, while that one in the high frequency domain looks very much flattened suggesting the presence of two semicircles. In early stages of both cells three processes can clearly be identified in the DRT. In late stages of aging the DRT of the 4.2 V-cell (Fig. 7a) is strongly increased as

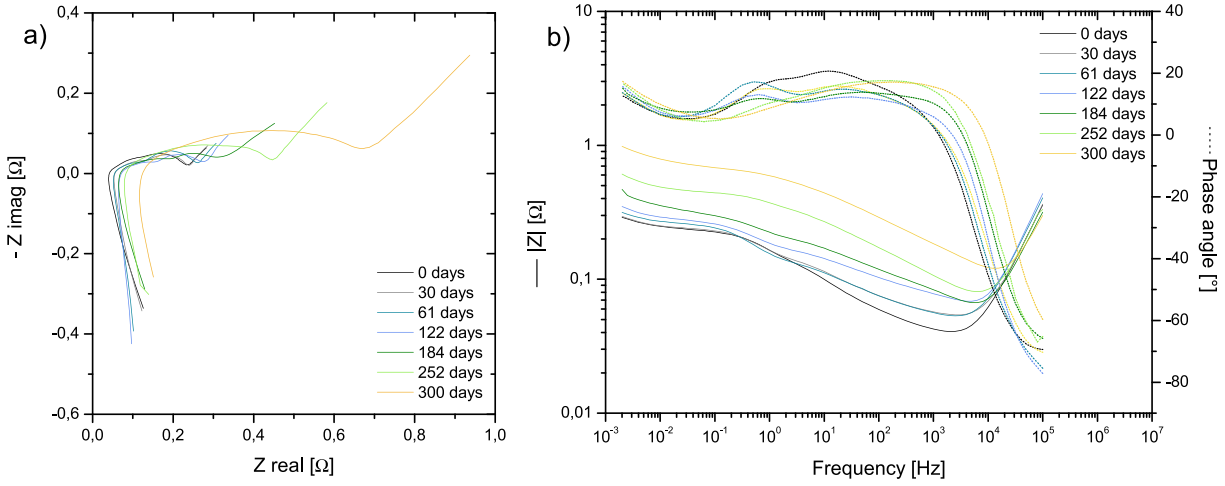

Fig. 4. Impedance spectra of calendar aged cell at 4.2 V and 60 °C after every 20 days. All spectra are taken at SOC10 at 0 °C.

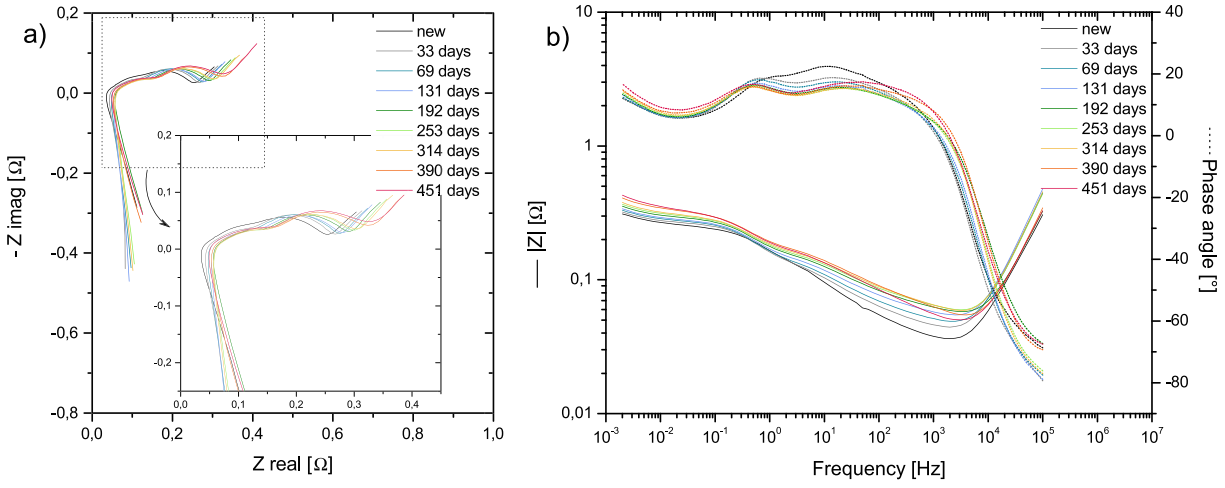

Fig. 5. Impedance spectra of cycle aged cell at 4.0 V and 60 °C after every 20 days. All spectra are taken at SOC10 at 0 °C. The cells have been aged for different durations. Same colors in the EIS spectra represent same aging durations. (For interpretation of the references to color in this figure legend, the reader is referred to the web version of this article.)

we could see in the impedance spectra of Fig. 4, while the DRT curves of the 4.0 V-cell (Fig. 7b) remains similar. Additionally at both cells a visible shift of the frequency in the peak between 10^2 and 10^3 Hz is observed. This peak is strongly influenced by the inductive behavior of the cell at higher frequencies. However for an inductive behavior the DRT cannot be used to describe the cell behavior sufficiently. The wide range of influence of the inductivity can be seen in the high residuals of the DRT in Fig. 7c and d. The residuals remain significant until ~40 Hz (marked as a dashed line), although the point of intersection of the EIS curve with the *x*-axis is ~10^3 Hz. The inductivity arises from the windings of the collectors, which do not change during aging, and the measurement cables, showing a current dependant coupling inductivity. During aging the cell's impedance increases leading to a lower current response during the measurement. A lower current causes a lower coupling of the measurement cables and thus a weaker magnetic field. This effect pretends smaller time constants for the high-frequency process resulting in a shifted peak to higher frequencies, because capacitive processes can now be realized at higher frequencies. In consequence this shift to higher frequencies should not be interpreted physically and is considered to be the result of the inductive coupling and of the pseudo-potentiostatic measurement mode.

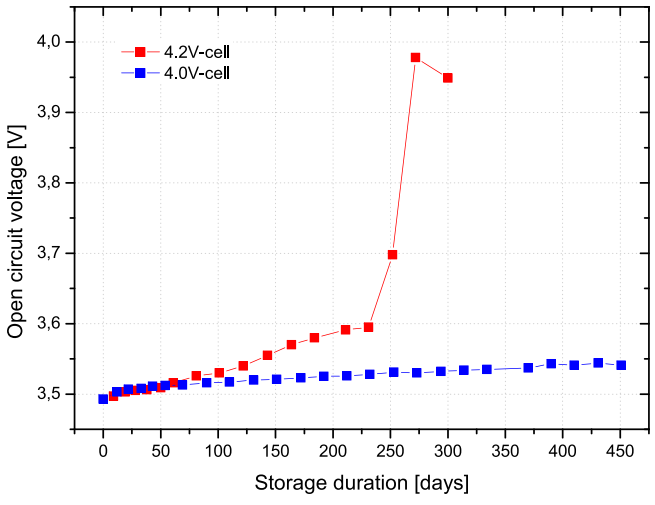

Fig. 6. Evolution of open circuit voltage at SOC10 during storage at 60 °C.

From our previous work [13] we know that the following processes may occur in the spectra: particle-current collector contacts (which are overlain by the inductive behavior of the cell in the high-frequency domain of the impedance spectra), SEI layer, charge-transfer processes of anode and cathode. Together with the information from the DRT the following equivalent circuit has been developed (Fig. 8).

The equivalent circuit consists of an RL parallel combination, a resistance R_{el}, two RQ elements and a transmission line model TLM. *L* represents the inductivity from the windings in the cell and the measurement cables, R_{el} describes the ohmic resistance. RQ_{SEI} stand for the process appearing in the high-frequency range, which is a part of the anode and is probably the response of the SEI layer. The second RQ element describes the charge transfer process of the anode. Sometimes, especially in early stages of aging, the SEI process may be overlapping with the charge-transfer process of the anode. The $TLM_{Cathode}$ is used to model the charge-transfer process of the cathode, which fits the response of the cathode best as will be seen later (Fig. 17). Constant phase elements are used to describe the porous electrode in its best way. The fitting has been conducted over a limited frequency domain. Only a small part of the inductive tail (at <15,800 Hz) has been considered in the fitting. Due to the free adjustment of the cell and measurement cables, differences in the shape of the inductive tail appear. As the observed frequency region does not comprise the diffusion, it has also not been considered in the evaluation of the impedance spectra. The impedance spectra have been fitted in ZView and the obtained resistance values are plotted in Fig. 9.

A detailed consideration on appearing effects at the single electrodes in symmetric arrangement will be shown later at the post-mortem analysis. The last three impedance spectra of the 4.2 V-cell are not present in Fig. 9, because the fit was unstable.

In both cases of aged cells the serial resistance (yellow line (in the web version)) increases slightly over the whole storage duration. It looks like the aged anodes (red line) show a very flat curve progression but on closer examination it can be seen that the resistances are slightly decreasing. Opposite to that the resistances for SEI layer and cathode charge-transfer resistance are increasing. Especially the SEI resistance (green line) of the 4.2 V-cell is drastically increasing at storage >125 days indicating a more distinctive SEI layer (see Fig. 13). Both aged cathodes (blue line) exhibit

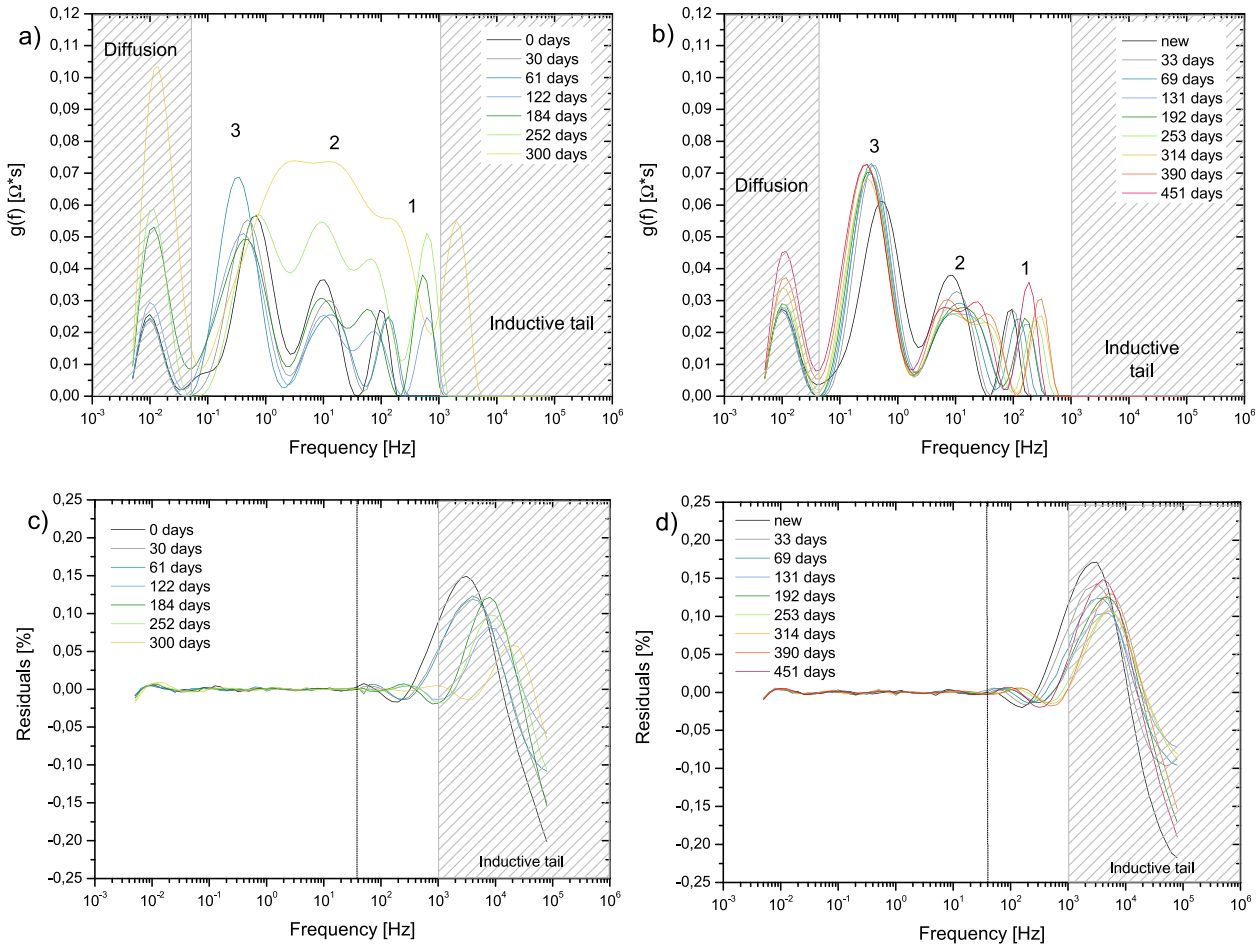

Fig. 7. DRTs calculated from EIS measurements (shown in Figs. 4 and 5) of a) the 4.2 V-cell and b) the 4.0 V-cell and corresponding residuals of the calculated DRT of c) the 4.2 V-cell and d) the 4.0 V-cell.

increased charge-transfer resistances, whereas the 4.2 V-cathode has a steeper slope of the curve than the 4.0 V-cathode. A reliable statement on changing resistances due to aging effects can only be done at the same potential of the anode and the cathode, but in the 18650 cell, at SOC10 the potential at the electrodes changes due to loss of cycleable lithium. Impedance spectra are then taken at undefined electrode potentials (of the cathode as well as of the anode). The effects of aging are thus overlapped to the effect of a changing potential at the electrodes. Due to this reason and the fact that during fitting the processes cannot be separated well, which makes fitting a real challenge, symmetric cells are built to investigate the electrodes separately. The fitted values of the 18650 data may give a trend at OCVs close to the new state, but with increasing aging duration the values are not any more representative.

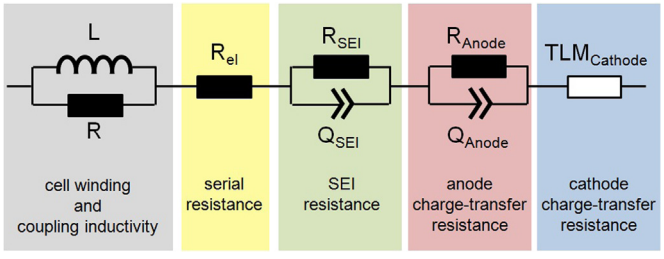

Fig. 8. Equivalent circuit to fit impedance spectra of the 18650 cell.

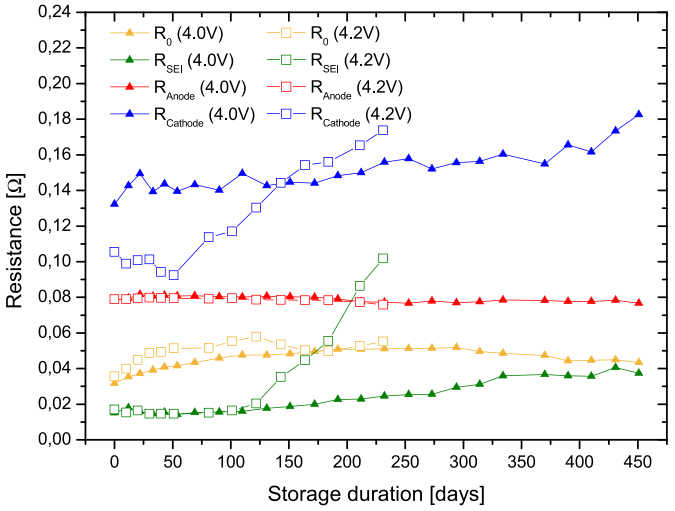

Fig. 9. Resistance values of fitted impedance spectra of 4.2 V-cell and 4.0 V-cell. R_0 = serial resistance, R_{SEI} = SEI resistance, R_{Anode} = anode charge-transfer resistance, $R_{Cathode}$ = cathode charge-transfer resistance.

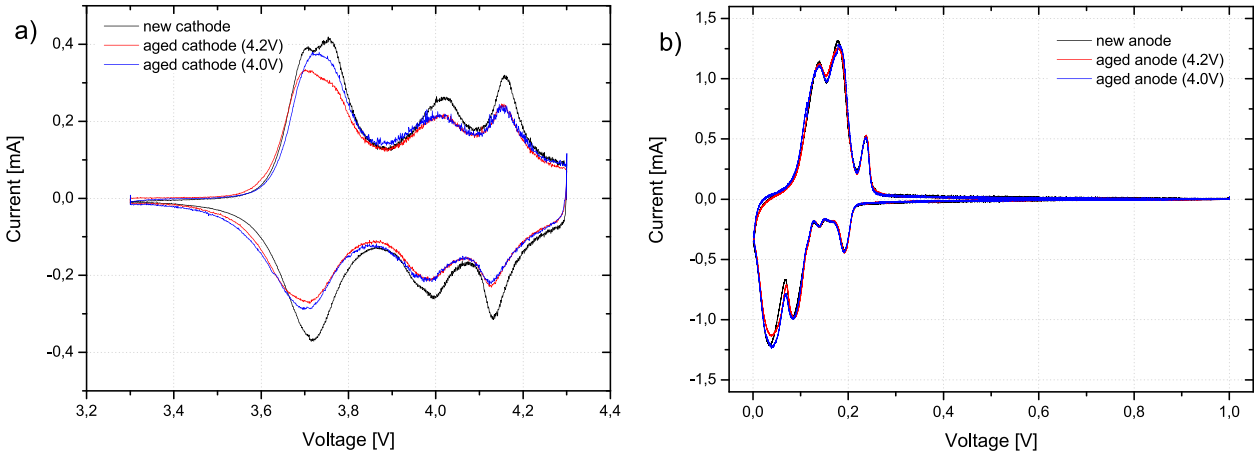

Fig. 10. Slow-scan cyclic voltammetry of new and aged a) cathode and b) anode, scan-rate: 5 μV s^{-1}.

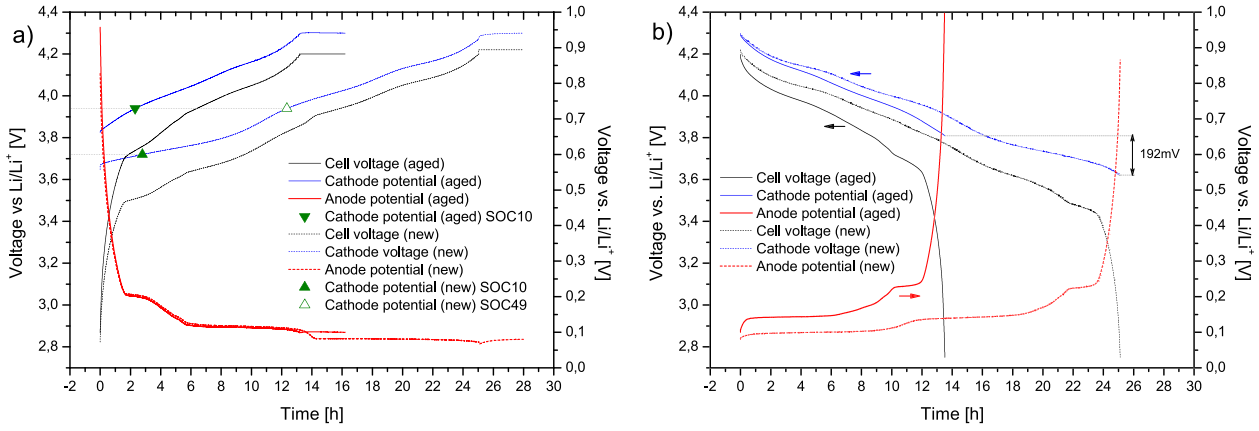

Fig. 11. Potential curves of new (dashed line) and aged (solid line) full cell, black curve: cell voltage, blue curve: cathode potential, red curve: anode potential of cell aged at 4.2 V and 60 °C at a) charging and b) discharging. (For interpretation of the references to color in this figure legend, the reader is referred to the web version of this article.)

As a first conclusion it can be said, that the reduction of the storage voltage of already 200 mV from 4.2 V to 4.0 V shows a drastic improvement concerning the 18650's:

- Capacity fade
- Power and inner resistance
- Increase in ohmic resistance due to increase of electrolyte's resistance

3.4. Electrochemical investigation of the aged cells

Slow-sweep electrochemical analysis at a discharge rate of C/50 has been conducted at aged cathodes and anodes to determine the capacity loss caused by loss of active material (e.g. isolated particles or transition metal dissolution). Discharge capacities at higher discharge rates may be highly influenced by the increase of the inner resistance and thus do not give information only about loss of

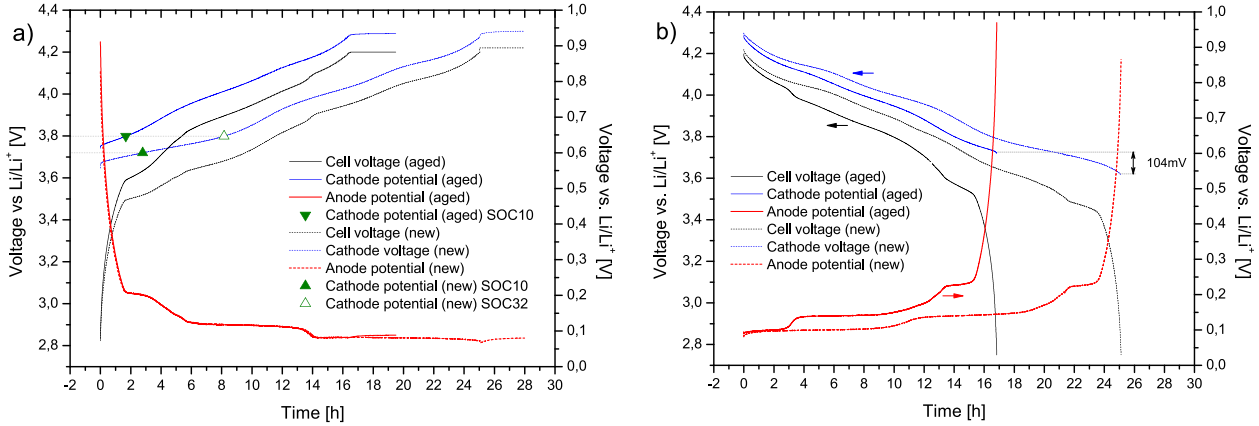

Fig. 12. Potential curves of new (dashed line) and aged (solid line) full cell, black curve: cell voltage, blue curve: cathode potential, red curve: anode potential of cell aged at 4.0 V and 60 °C at a) charging and b) discharging. (For interpretation of the references to color in this figure legend, the reader is referred to the web version of this article.)

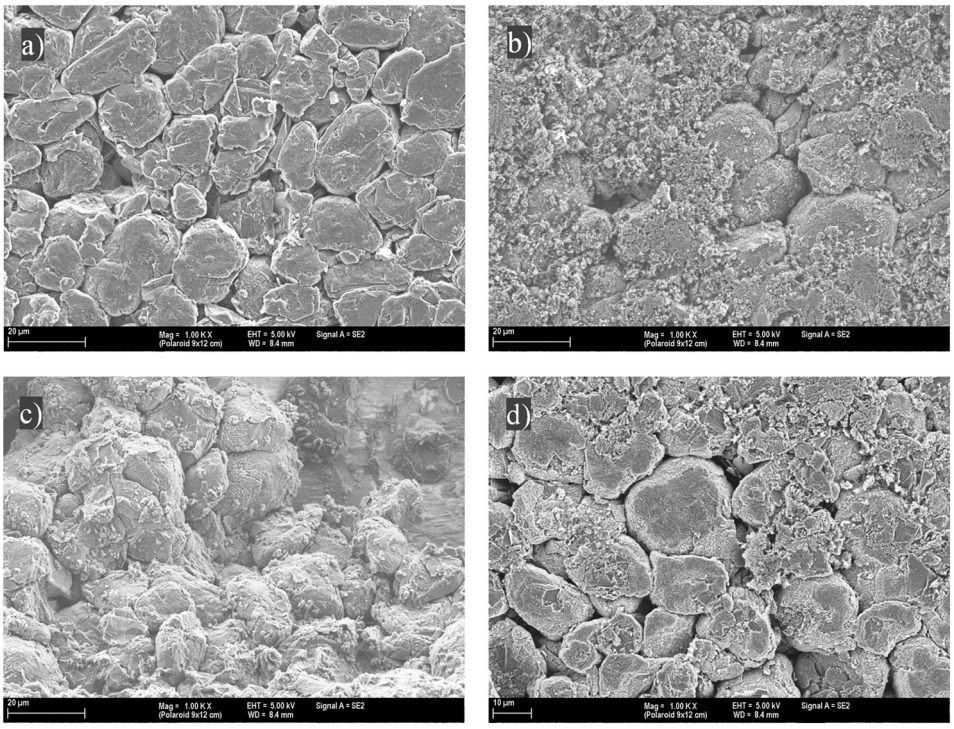

Fig. 13. Comparison of a) new, b) 4.2 V calendar aged, c) fractured surface of 4.2 V aged and d) 4.0 V aged anodes.

active material. The following Table 1 gives an overview of the capacity of new and aged electrodes and the attributed mechanisms of capacity loss.

These measurements allow us to estimate the capacity loss from active material loss, which is about 5.1% for the 4.2 V-cathode and 3.5% for the 4.0 V-cathode. The aged anodes show a capacity fade of 2.3% and 1.9% at C/50 indicating an even lower value of active material loss at the anode than at the cathode. Due to the overdimensioning of the anodes (about 8% higher capacity in comparison to the cathode in the new state), it is not assumed that the small loss of anode active material has an influence on the total capacity loss of the 18650 cells. Compared to the total capacity loss of the 18650 cell, also the capacity fades from the cathodes due to active material loss or isolated particles only take a minor part in both cells. Comparing the capacity value for the C/10 and 1C discharge it is clear from Table 1 that the capacity fade is significantly higher than for the C/50 discharge, indicating that the electrodes reveal a higher overall resistance. This is valid for both, the cathode and the anode, but the cathodes show this effect more distinctive. This indicates that the resistance on cathode side is much more influenced by the aging than on the anode side.

Slow-scan cyclic voltammetry has been conducted at the aged anode and cathode (see Fig. 10). Both cathodes show a reduced peak height at the position of the NMC (~3.7 V) and the spinel (~4 V, 4.15 V peaks) compared to the new state, which means that both parts of the blend cathode suffer from loss of active material (e.g. by transition metal dissolution or isolated particles). The extent of the peak height reduction at the NMC peak is smaller at 4.0 V than at 4.2 V and nearly equal at the position of the $LiMn_2O_4$ peaks. This is in accordance to the already shown slow-sweep electrochemical analysis, where the 4.2 V cathode exhibits a higher capacity fade compared to the 4.0 V-cathode (see Table 1).

The 4.2 V- and 4.0 V-aged anodes (Fig. 10b) do not show significant differences compared to the new state, which suggests an almost retained initial capacity, which is also in agreement to the slow sweep electrochemical analysis shown in Table 1.

In the experiment shown in Figs. 11 and 12 an EL-Cell with anode and cathode + metallic lithium reference electrode was charged with C/25 to 4.2 V, followed by a 3 h CV step at 4.2 V. The discharge was performed also at a rate of C/25 to 2.75 V. With the help of the reference electrode the potential of anode and cathode was monitored during charge and discharge. An EL-Cell with new electrodes (dashed lines) is compared to an EL-Cell made of aged electrodes (solid lines). The charge step is shown in Fig. 11a (4.2 V cell) and Fig. 12a (4 V cell), the corresponding discharge step in Fig. 11b (4.2 V cell) and Fig. 12b (4 V cell).

In case of the 4.2 V-cell (Fig. 11a and b) a reduced full cell capacity is apparently, which results in the fact that the voltage level of the aged cathode, and thus the aged full cell, changes significantly faster compared to the new cell. The voltage curves of the new and aged anode run at exactly the same potential, but the lower plateau of the aged graphite vs. lithium curve is not used to full capacity as the dashed line shows it for new graphite vs. lithium. As half of the graphite's capacity is stored at the lower plateau, this graph shows that nearly half of the graphite's capacity is not utilized in the cell's aged condition. This phenomenon can be constituted to a minor extend by loss of active material (which is only 5% for the cathode) but mostly by loss of cycleable lithium. During charging and storage at high voltages lithium is irreversibly consumed in side reactions like SEI layer growth on the anode. This effectively is the reason why the cathode cannot be fully lithiated during discharge and is therefore at a more positive potential in the discharged state. Consequently the anode is also at a more positive potential in the discharged state. The potential difference is charted in Fig. 11b and is 192 mV.

Fig. 12 discloses a quite similar shape of the potential curves. In case of the 4.0 V cell the total cell capacity is diminished as well, but to a smaller extent compared to the 4.2 V-cell. This is very well in agreement with the capacity fade shown in Fig. 1 for the 18650 cells. Thus the lower plateau of the aged anode (Fig. 12a) is partially filled, indicating a smaller capacity fade, due to consumption of cycleable lithium for SEI layer formation. Nevertheless, also within

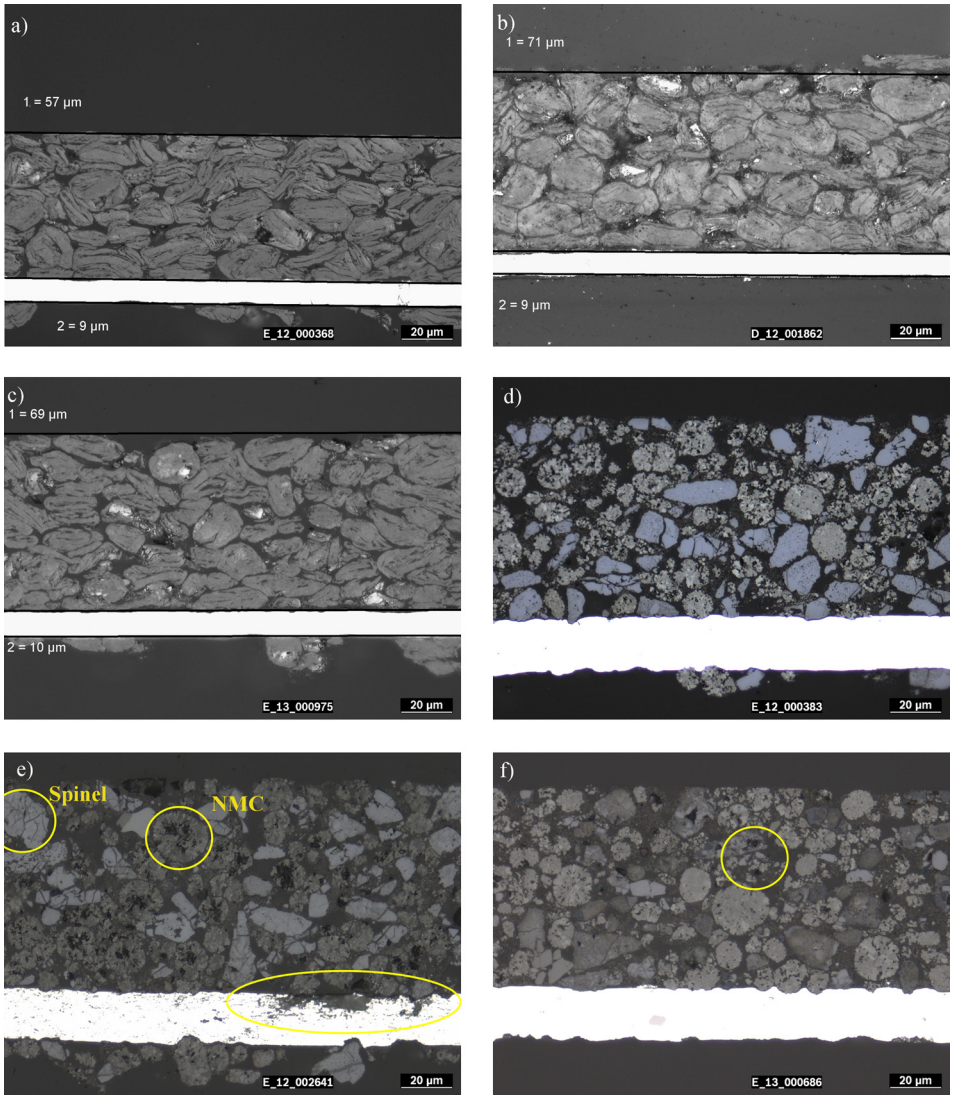

Fig. 14. Light microscopy images of cross-section polish of a) new anode b) 4.2 V aged anode c) 4.0 V aged anode d) new cathode e) 4.2 V aged cathode f) 4.0 V aged cathode.

the cell aged at 4.0 V the major part of the capacity loss is the irreversible consumption of lithium due to SEI layer formation at the anode, which limits the cathode to be fully charged. A potential difference of 104 mV between new and aged cathode is observed in this case as drawn in Fig. 12b.

Out of these schemes the changing shape of the impedance spectra in Figs. 4 and 5 can be explained. Within Figs. 11 and 12 green triangles mark certain positions, which should be regarded when evaluating the impedance spectra. In Figs. 4 and 5 the impedance spectra are measured at SOC10. The green filled triangle

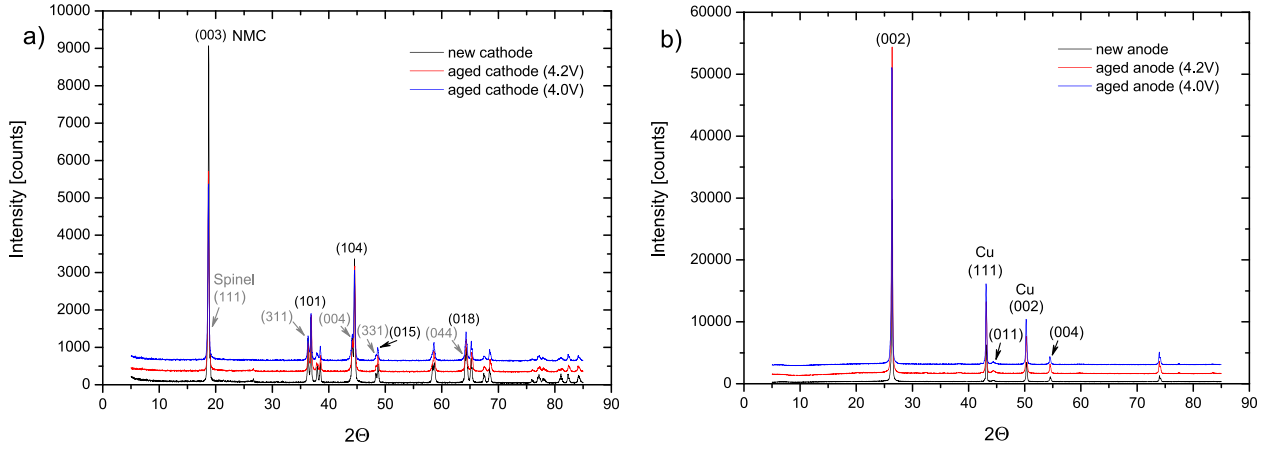

Fig. 15. XRD pattern of new and aged a) cathode and b) anode.

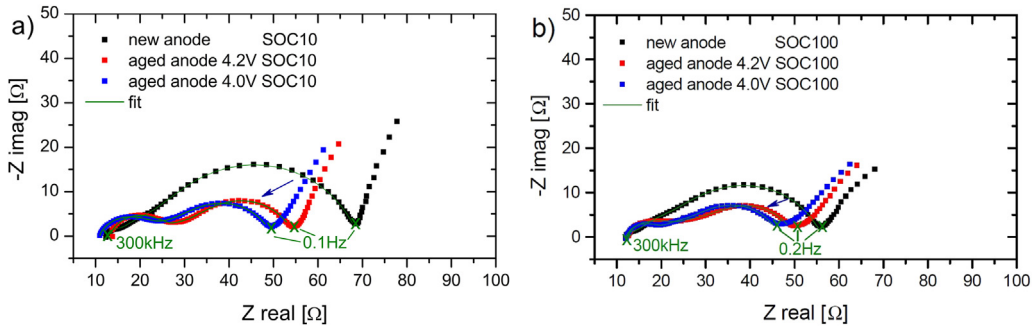

Fig. 16. Impedance spectra of new and aged anodes at a) SOC10 and b) SOC100 in Nyquist plot of the 4.2 V and 4.0 V aged cell at 60 °C. The overall impedance of the aged anodes decreases.

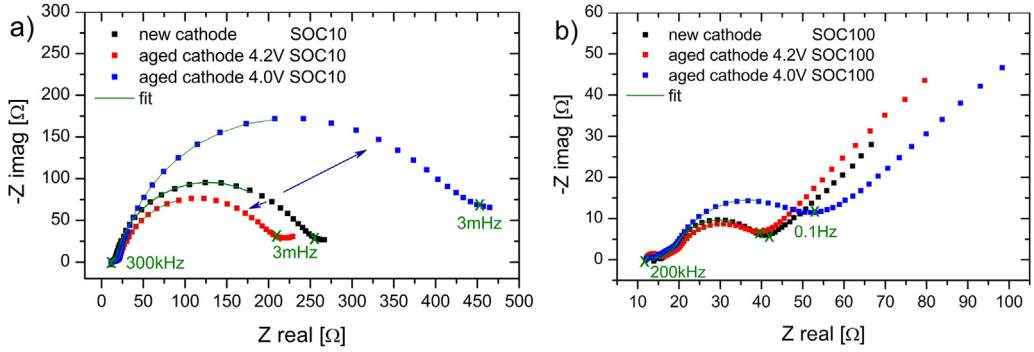

Fig. 17. Impedance spectra of new and aged cathodes at a) SOC10 and b) SOC100 in Nyquist plot of the 4.2 V and 4.0 V aged cell at 60 °C.

in the blue dashed line of Figs. 11 and 12 mark the potential of the cathode at SOC10. With loss of active material and cycleable lithium the corresponding cathode potential at SOC10 in the aged state is shifted (marked by the filled green triangle at the solid blue line). Comparing the cathode voltage at SOC10 in the new and aged state reveals a difference of 100–200 mV and thus a completely different SOC of the cathode in its new state (unfilled green triangle). Due to the sensitivity of the cathode upon voltage variation [13] a mixture of aging and voltage-variation is measured in the EIS of the aged 18650 cell. In principle the anode is relatively insensitive against potential variation (between SOC10 and SOC100) as shown in our previous paper [13], but due to loss of cycleable lithium the potential of the anode at SOC10 shifts to higher potentials (in direction to SOC0). Decreasing the potential in this direction might have a significant influence on the anode's impedance spectra, which can be seen in an increase of the fitted data of the 18650 cell.

At this point one can conclude that the main reason for the capacity fade is loss of cycleable lithium for SEI layer formation. Although loss of positive active material is more pronounced at the 4.2 V-stored cell (see later) it adopts only a minor part. The rate

Table 1
C/50, C/10 and 1C capacities of new and aged electrodes, showing the capacity loss due to active material loss and due to increase of inner resistance (at 1C). Each of the three quoted values are from three different cells.

	C/50 Capacity [mAh cm^{-2}]			Ø Capacity loss by active material loss [%]		C/10 Capacity [mAh cm^{-2}]			Ø C/10 Capacity loss [%]	
	New	4.2 V aged	4.0 V aged	4.2 V aged	4.0 V aged	New	4.2 V aged	4.0 V aged	4.2 V aged	4.0 V aged
Cathode		2.728	2.774				2.600	2.663		7.3
	2.899	2.726	2.790	5.1	3.5	2.877	2.600	2.668	9.8	
		2.715	2.764				2.587	2.672		
Anode		3.062	3.041	2.3	1.9	3.122	2.997	3.028		
	3.126	3.055	3.078				2.995	3.057	4.1	2.7
		3.044	3.079				2.993	3.030		

	1C Capacity [mAh cm^{-2}]			Ø 1C Capacity loss [%]	
	New	4.2 V aged	4.0 V aged	4.2 V aged	4.0 V aged
Cathode		2.111	2.089		
	2.564	2.115	2.075	17.9	18.2
		2.093	2.125		
Anode		2.824	2.888		
	3.061	2.812	2.935	8.1	5.1
		2.802	2.887		

Table 2
Lattice parameter of new and aged anodes and cathodes.

Electrode	$a_{Graphite}$ [Å]	$c_{Graphite}$ [Å]	$a_{Spinell}$ [Å]	a_{NMC} [Å]	c_{NMC} [Å]
New anode	2.46(2)	6.71(2)	–	–	–
Aged anode (4.2 V)	2.46(1)	6.71(3)	–	–	–
Aged anode (4.0 V)	2.46(1)	6.71(0)	–	–	–
New cathode	–	–	8.21(8)	2.86(4)	14.26(3)
Aged cathode (4.2 V)	–	–	8.20(8)	2.85(8)	14.29(1)
Aged cathode (4.0 V)	–	–	8.20(9)	2.86(1)	14.28(1)

capability tests also mainly show the increase of the cathode's resistance and at a smaller extent the anode's resistance.

3.5. Materials analysis of the aged cells

The surface of the electrodes has been investigated by SEM and EDS analysis. Comparing new and aged cathodes does not show large differences in their visual nature. Therefore no images are shown here.

Comparing Fig. 13a with Fig. 13b shows intensive formation of a surface layer at the anode's surface of the 4.2 V-cell. At some positions the initial surface emerges beneath the surface layer. During disassembling of the 18650 cell the separator has to be removed from the surface of the anode. In the aged state the separator can only be removed with increased effort. It is not clear if parts of this surface layer stick to the separator and are thus detached unintended. Assuming that this surface layer is not the SEI but an additional layer (formed e.g. from decomposition products of the electrolyte), which is permeable for the whole electrolyte, this layer would act as an additional barrier leading to an increased ohmic resistance. The increase of the ohmic resistance (Figs. 4 and 5) cannot only explained by the decomposition of electrolyte. Considering diagrams of specific conductivity as a function of the amount of the conductive salt will support this theory. If the electrolyte's conductivity is reduced by a factor 1.5 the amount of the conductive salt should be reduced by 65%, which is not realistic. Assuming that not only $LiPF_6$ decomposition takes place but as well organic solvent decomposition leads to the fact that even more $LiPF_6$ has to be decomposed to diminish the electrolyte's conductivity by a factor 1.5. This could explain the massive increase of the inner resistance shown in Fig. 2 for the 4.2 V-cells. It is interesting to see that at the fractured surface of the aged anode (see Fig. 13c), the pristine shape of the graphite particles can be seen. But even at these particles one can see the incipient layer formation as all particles show partially covered areas. The 4.0 V-anode in Fig. 13d shows less layer formation after 451 days storage at 60 °C, but keeping in mind that this might originate from the removal of the separator. Nevertheless it seems to be that the formation of the layer starts partially at different positions and not comprehensive over the whole surface.

EDS analysis proved the presence of manganese, nickel and cobalt at the surface of the 4.2 V-anode, but only manganese at the surface of the 4.0 V-anode. So far irreversible loss of cycleable lithium due to consumption for SEI layer growth has been extracted to be one of the main aging factors. A higher amount of transition metals are found on the 4.2 V-anode's surface. Together with the results of the potential test (Figs. 11 and 12) we believe that the 4.2 V-cell develops a more distinctive SEI layer. This leads us to the assumption that a higher amount of transition metals on the anode causes an accelerated SEI layer growth. Additionally the SEI layer is instable when exposed to elevated temperatures, which is another factor for continuous lithium consumption and thus capacity fade as the layer is continuously rebuild [15].

Table 3
Concentrations of transition metals in new and aged anode.

Electrode	Mn [mg kg^{-1}]	Ni [mg kg^{-1}]	Co [mg kg^{-1}]
New anode	136	53	35
Aged anode (4.2 V)	936	213	94
Aged anode (4.0 V)	320	130	67

Light microscopy images of cross-sections of aged electrodes showed that the aged anodes strongly increased in thickness from 57 μm (new) to 71 μm (4.2 V-aged) and 69 μm (4.0 V aged). It seems to be, that the particles extended in size. One possible explanation would be the occurrence of an SEI layer around each particle, as the electrolyte penetrates the whole electrode and thus the layer is able to from at all surfaces. In case of the 4.2 V-anode the sharp and clear boundaries of the graphite particles are vanished. Contrary to that the structure of the 4.0 V-aged anode after grinding and polishing looks in between that of the new and 4.2 V-aged cell. In Fig. 14a and c the typical lamellar structure and intact particles can be observed, which are hardly visible in Fig. 14b.

The 4.2 V-cathode exhibits distinct aging phenomena. Firstly current collector corrosion appears (see mark in Fig. 14e), probably due to HF attack, which could be built intrinsic by reaction of traces of water with the $LiPF_6$ containing electrolyte. Augmented particle fracture, especially in the case of the spinel particles can be seen as marked in Fig. 14e. The primary particles of the $Li(Ni_{0.5}Mn_{0.3}Co_{0.2})O_2$ phase are loosened, which can be easily seen in Fig. 14e where black areas within NMC particles indicate break loosened primary particles vanishing during grinding and polishing of the materialographic specimen. Both breaking of spinel and loosened primary particles of NMC can cause small loss of active material seen in the slow-sweep electrochemical analysis (Table 1).

In case of the 4.0 V-cell small variations compared to the new cell can be detected. As already seen at the 4.2 V-cell also the cathode of the 4.0 V-cell shows loosened NMC-particles, which is in evidence at the black areas inside the NMC particles. But the amount of these areas is much less than in case of the 4.2 V-cell. Cracks inside spinel particles do not occur frequently. Usually cracks appear during cycling, which has not been done in these experiment (except a few intermediate measurements). The free space in the battery housing is very limited. During storage, the surface layer is growing continuously as seen in Fig. 13. The remarkable increase of the anode layer may exert pressure over the whole length of the jelly roll and probably causes cracks within the cathode particles.

To see how the materials have changed during storage at elevated temperatures X-ray diffraction pattern are taken from new and aged anode and cathode. The electrodes are discharged at C/50 to SOC0 and afterward measured under argon atmosphere. The aged anode does not show differences in its peak pattern compared to the new cell as can be seen in Fig. 15b and the values of Table 2.

The aged cathodes however show changes in the lattice parameters of $LiMn_2O_4$ and $Li(Ni_{0.5}Mn_{0.3}Co_{0.2})O_2$. The lattice parameter a_{NMC} of the 4.2 V-cell slightly decreases, c_{NMC} increases. As already described in our previous paper [13] the loss of transition metals by dissolution into the electrolyte causes a decreased amount of lithium inside the lattice. Because less Li^+ can be intercalated into the structure the average oxidation number of the transition metals is higher, than in the fully intercalated state, leading to a stronger interaction with the negatively charged oxygen ions and thus a decrease of the interlayer distance represented by parameter c. The typical behavior of NMC with different lithium amounts [13,17] confirms this theory. a_{NMC} of the 4.0 V-cell stays nearly constant, while c_{NMC} shrinks slightly as well. The amount of shrinkage is smaller than for the 4.2 V-cell, which is in accordance to the results from cyclic voltammetry. The lattice parameter $a_{Spinell}$ slightly shrinks in both aged cases, which is in accordance to Liu

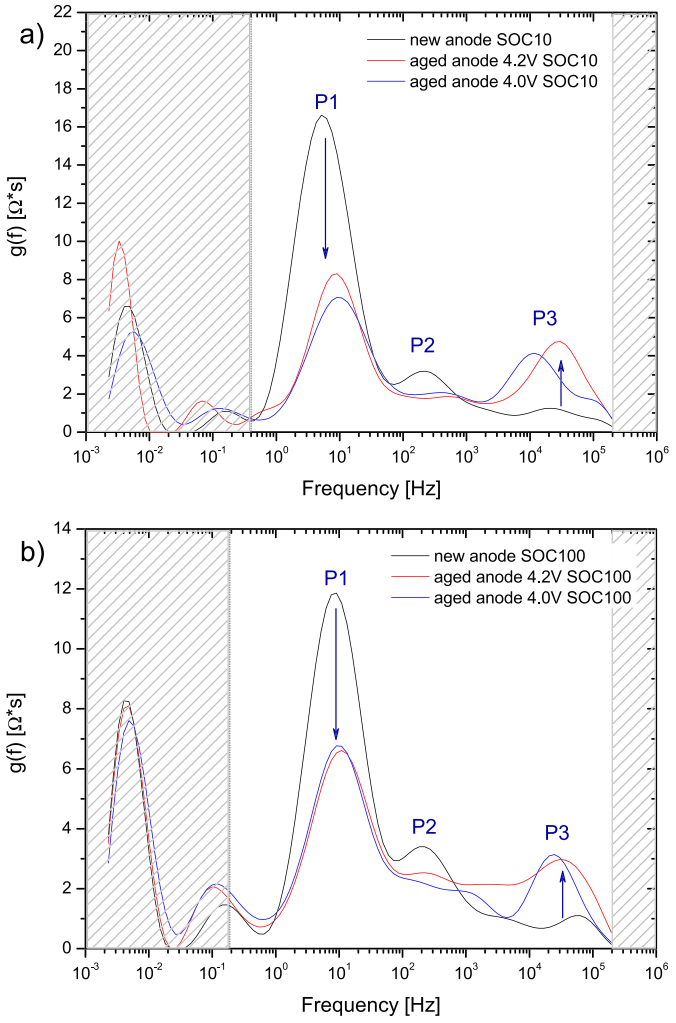

Fig. 18. DRTs calculated from EIS measurements (shown in Fig. 16) of the anode at a) SOC10 and b) SOC100. Gray shaded regions mark non-evaluable areas. Both DRTs show reduced impedances, as already seen from the impedance spectra in Fig. 16.

et al. [18]. The shrinkage may be also caused by loss of transition metals in the lattice and thus a decreased amount of lithium ions, which is as well in accordance to the cyclic voltammetry, where comparable peak heights of the 4.2 V and 4.0 V-cell could be seen.

Analysis of aged anodes by ICP-OES is another method to prove loss of active material of the cathode by transition metal dissolution. Transition metal dissolution was shown to be a relevant aging mechanism [4,15]. The following Table 3 lists the detected transition metal concentrations of new and aged anode. The list confirms the qualitative results from EDX measurements that the concentration of transition metals at the anode increases for the cell aged at a 4.2 V compared to 4.0 V.

Dissolution of manganese can be caused by two main reaction mechanisms in the cell [16], which can be due to disproportionation of Mn^{3+} to Mn^{2+} and Mn^{4+} ions at low states of charge, or due

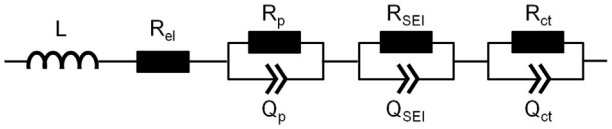

Fig. 19. Derived electrical equivalent circuit for new and aged anode at SOC10 and SOC100.

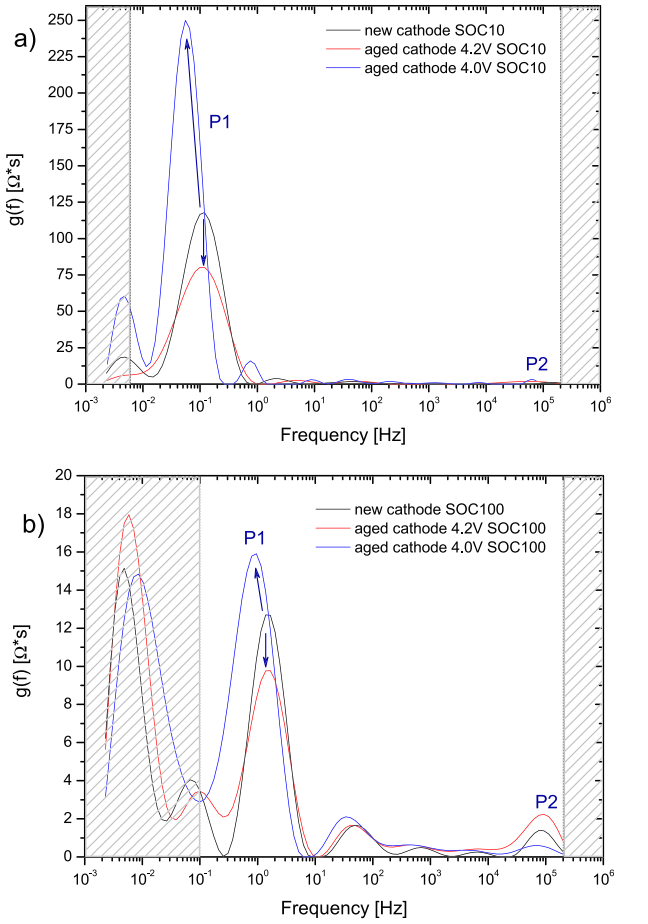

Fig. 20. DRTs calculated from EIS measurements (shown in Fig. 17) of the cathode at a) SOC10 and b) SOC100. Gray shaded regions mark non-evaluable areas.

to traces of HF within the electrolyte. At 4.2 and 4.0 V manganese has an oxidation number of approximately +4 in the spinel phase, where the Jahn–Teller distortion (appearing at low states of charge) is not pronounced. Because manganese ions do not change their oxidation state to Mn^{3+} within the NMC, manganese dissolution caused by HF is more likely, which is confirmed by the decrease in peak height of the NMC peak in the cyclic voltammetry. Additionally current collector corrosion, most likely by HF attack, was found supporting this theory. Ni and Co do not show disproportionation reactions, which suggest the dissolution by HF to be presumable. This mechanism is accelerated at elevated temperatures [4]. Dissolved transition metals are transported through the electrolyte to the surface of the anode and incorporate into the SEI layer [3,4,15,19] leading to an increased SEI layer growth and loss of cycleable lithium as shown in Figs. 11 and 12. Additionally the electronic conductivity of the SEI may be increased by these metals [5]. The higher amount of transition metals at the 4.2 V-anode and thus a higher loss of cycleable lithium (Fig. 11) could be confirmed. Loss of electric contact and thus isolated particles remains to be another reason for loss of active material.

3.6. Investigation of the aged cell by impedance spectroscopy and DRT

Electrochemical impedance spectroscopy has been conducted on aged anodes and cathodes in symmetric cells at defined potentials. Because the electrodes are very sensitive to voltage changes [13], it is necessary to set new and aged cells at the same

potential as e.g. SOC10 may be at a different voltage in the aged state, due to capacity loss, compared to the new one (see Figs. 11 and 12). In the following figures the curves are denominated with SOC10 and SOC100 which refers to potentials of the electrodes at SOC10 and SOC100 of a new cell. Kramers–Kronig residuals have been calculated representing the quality of the measured impedance spectra. The data quality of the measured impedance spectra is very good, indicated by the Kramers–Kronig residuals below 0.5%. For the aged and new cathode at SOC10 and 0 °C residuals above 1% could be observed. This can be attributed to a slightly time invariant behavior affecting measured frequencies below 1 Hz. As the regarded frequency range for analysis is limited to higher frequencies, the measurements could be included in the analysis.

Figs. 16 and 17 show the measured impedance spectra of new, 4.2 V-aged and 4.0 V-aged anodes and cathodes at SOC10 and SOC100, respectively.

In Fig. 16a and b it can be clearly seen that the charge-transfer resistance of the aged anode (low-frequency semi-circle) is reduced compared to the new one. This trend is present for SOC10 and SOC100. Particle-current collector contacts, predominantly appearing in the high-frequency domain of the impedance spectra significantly increased, which could be due to the difficulty described in chapter 2.3, when the coating tends to flake off during reassembling the EL-Cells from half cells to symmetric cells. Therefore the increase in the high-frequency domain is not representative for an exclusive variation in particle-current collector contacts.

Contrary to the aged anode the cathode shows ambivalent results. The 4.2 V-cathode shows a decrease in its charge-transfer resistance, while the 4.0 V-cathode increases remarkably, marked in Fig. 17a and b. Again SOC10 and SOC100 show the same trend. The high-frequency semi-circle, again corresponding to particle-current collector contacts increases slightly, indicating a worse adhesion compared to the new state.

Figs. 18a and b and 20a and b show the calculated DRTs in order to derive a physically interpretable equivalent circuit model to fit the shown impedance spectra.

In Fig. 16a and b two well separated semi-circles can be seen. Both semi-circles, especially the low-frequency arc, look very much flattened, thus indicating an overlap of two processes or non-ideal behavior of the occurring capacitances. Fig. 18a and b discloses three well separated main peaks in the frequency range between 200 kHz and 0.2 Hz. Frequencies <0.2 Hz cannot be interpreted properly by the DRT method without using a pre-processing step. For frequencies >200 kHz the evaluation is limited by the inductive behavior of the measured system arising from the coupling inductivity of the measurement cables. These non-evaluated parts of the impedance spectra are marked as gray shaded areas in Figs. 18 and 20. With the information from the DRT the generation of the following electrical equivalent circuit (see Fig. 19) ensued.

The equivalent circuit consists of an inductor L, a resistor R, three RQ-elements. RQ elements are used instead of RC elements to describe the porous nature of the electrodes in the best way. L represents the inductivity from the measurement cables and R_{el} describes the ohmic resistance. RQ_p stand for the process appearing in the high-frequency range, which is probably a particle-current collector contact resistance [18]. The second RQ element describes processes from SEI layers, which are often partially overlapping with the following charge-transfer process. The third RQ models the charge-transfer process in the mid frequency domain. As the observed frequency region does not comprise the diffusion, it can be discounted. The impedance spectra have been fitted in ZView and the obtained values are listed in Table 4.

The main peak in Fig. 18 (marked as 1) is located at a frequency of 10 Hz and decreases for both types of aged anodes, corresponding to a decrease in the overall charge-transfer resistance. The peak frequency of the process stays the same according to an unaltered time constant and thus an unchanged material. As already described in our previous paper [13] a reduced charge transfer resistance can be reasoned by an increased surface inside the material. An increasing surface can also be the reason for the increasing charge transfer capacitances C_{ct} in Table 4. Exfoliated graphene layers or cracked particles might be the reason for an increased surface in the aged state. The observations from the symmetric cells are in accordance to those of the 1850 cells where as well a reduced anode charge-transfer resistance could be seen. To prove this phenomenon 3D microstructure reconstruction based on μ-CT images, where a wide range of microstructural parameters can be calculated are in progress.

The second peak, appearing at 200 Hz, refers to the SEI layer at the surface of the graphite particles [19]. The aged anodes exhibit reduced SEI resistance, which is at first sight not consistent to the assumption of a thickened SEI after aging. Theoretically the impedance in this frequency domain is expected to increase, at least for the 4.2 V-aged anode, due to the presence of a highly distinctive SEI layer found in the SEM images (Fig. 13). From the literature [15] it is well known that the SEI layer is continuously growing during storage at elevated temperatures, because the SEI breaks, partially dissolves and rebuilds. Effectively the fitting values of R_{cl} of all aged anodes decrease which may have different reasons. However we assume that the most influential effect is the preparation step before measuring the impedance has also to be taken into account. The values have to be considered critically, because the SEI is definitely changed during removing of the electrodes from the 18650 cells, where the layer typically runs dry. Mechanical stress during preparation might also change the SEI layer e.g. the layer is partially demolished and thus the resistance decreases. Because the curves of SOC10 and SOC100 are measured at two different cells small variations during the preparation (e.g. preparation time, hardness of mechanical stress) may have an influence on the shape of the SEI layer and may cause differences in the DRT.

Peak 3, corresponding to particle-current collector contacts appears at frequencies between 10^4 and 10^5 Hz. In both cases of aged cells a remarkable increase of the peak height has to be noted. This peak is as well as the SEI layer highly influenced by the preparation step. In our previous paper [13] we already discussed extensively the influence of the preparation step. The coating of the aged anodes tends to flake off the current collector and these delaminated regions highly affect the appearance of this process, which can be seen in the high frequency area of Fig. 16 and in the values of Table 4.

The results from EIS enable us to further interpret the results from the rate capability test. There it was shown that the rate capability at higher rates is decreased indicating an increased overall resistance. On the other hand EIS deliver a reduced charge-transfer resistance. This leads us to the assumption that the aged anodes suffer from a worse diffusion inside the electrode. Light microscopy images already disclosed that the lamellar structure of the new graphite vanished in the aged state, which might be caused by pore clogging increasing the diffusional resistance.

Fig. 20a and b shows the calculated DRT of new and aged cathodes. In the Nyquist plot of Fig. 17a and b one very small high-frequency and one dominant low-frequency semicircle can be observed. These two semicircles are connected by a line at an angle of about 45°. The impedance spectrum with this shape can be described in its best way by the transmission line model (TLM) of Bisquert [20] for porous mixed phase electrodes. This thesis is supported by the shape of the calculated DRT where one dominant main peak and a few small side peaks appear, which is the characteristic pattern by the TLM. The main peak, marked as P1, is located around 0.1 Hz for SOC10 and 1 Hz for SOC10 and represents

Table 4
Values of fitted impedance spectra from Fig. 16. R = resistance, C = capacitance, n = QPE-specific variable $0.5 \leq n \leq 1$.

Electrode	SOC	R_p [Ω]	R_{SEI} [Ω]	C_{SEI} [F]	n_{SEI}	R_{ct} [Ω]	C_{ct} [F]	n_{ct}
Anode new	10	3.53	9.26	$9.61 \cdot 10^{-4}$	0.64	44.30	$1.52 \cdot 10^{-3}$	0.77
Anode 4.2 V aged	10	14.52	6.05	$1.37 \cdot 10^{-3}$	0.66	22.11	$2.46 \cdot 10^{-3}$	0.75
Anode 4.0 V aged	10	13.83	5.66	$1.76 \cdot 10^{-3}$	0.65	20.24	$2.48 \cdot 10^{-3}$	0.74
Anode new	100	3.36	9.07	$7.30 \cdot 10^{-4}$	0.67	32.61	$1.55 \cdot 10^{-3}$	0.75
Anode 4.2 V aged	100	13.18	7.08	$9.49 \cdot 10^{-3}$	0.69	18.97	$2.51 \cdot 10^{-3}$	0.74
Anode 4.0 V aged	100	8.63	6.88	$7.82 \cdot 10^{-3}$	0.70	19.94	$2.55 \cdot 10^{-3}$	0.74

the charge transfer resistance. In the frequency region >10 Hz the associated side peaks appear. At about 10^5 Hz one additional small peak P2 appears corresponding to the particle-current collector contacts in the cell.

Qualitatively the DRT shows the same trend as already seen in the measured impedance spectra. Surprisingly the 4.2 V-cathode is equal to the new state when measured at SOC100 and decreases its charge-transfer resistance compared to the new state when measured at SOC10. This is due to small differences in the OCV value of the symmetric cathode at SOC10 compared to the new state. The OCV value of the aged cathode was slightly higher than in the new state and due to the strong SOC dependency the overall impedance appears to be smaller in the aged state than in the new state. It can be assumed that the data from the measurement at SOC100 is close to the real relation between new and aged state. The 4.0 V-cathode showed a keen increase at both SOCs. Contemporarily the characteristic frequency remained constant for the 4.2 V-cathode and slightly decreased in case of the 4.0 V-cathode. The trend is obvious at both measured SOCs.

With this result of the DRT the corresponding electrical equivalent circuit can be built as shown in Fig. 21.

L, R_{el}, and RQ_p again describe the inductivity of the measurement cables, the ohmic resistance and particle-current collector contacts. The TLM represents charge transfers coupled with the electrolyte conductivity in the pores. The equivalent circuit model again did not consider the diffusion tail. The fitted values are listed in Table 5.

Because the tortuosity and the electrochemical active surface of the aged cathodes are unknown, the length is fixed to 1 to achieve comparable values. From the fitting values it can be seen that the particle-current collector contact increases slightly probably caused by a worse adhesion after aging. The reduced peak height in the DRT for the 4.2 V-cathode is clearly seen in the fitting values for R_{ct}, the time constant τ is in the same dimension as the new electrode. Respectively R_{ct} and the time constant for the 4.0 V-cathode are increased. An increased charge-transfer resistance of the 4.0 V-cathode can be confirmed by fitting results from the 18650 cell. The reason for the contrary conclusions concerning the charge-transfer resistance of the 4.2 V-cathode between 18650 cell (increasing R_{ct}) and symmetric cells (decreasing R_{ct}) have to be investigated in further studies.

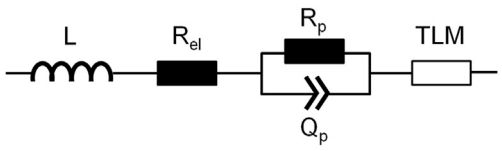

Fig. 21. Derived electrical equivalent circuit for new and aged cathode at SOC10 and SOC100.

Table 5
Values of fitted impedance spectra from Fig. 17. R = resistance, τ = time constant, n = TLM specific constant $0.5 \leq n \leq 1$, L = active length in TLM.

Electrode	SOC	R_p [Ω]	R_{ct} [Ω]	τ [s]	n	L
Cathode new	10	1.52	223.5	2.23	0.90	1
Cathode 4.2 V aged	10	4.29	186.7	2.57	0.88	1
Cathode 4.0 V aged	10	6.32	402.1	4.32	0.90	1
Cathode new	100	1.78	22.75	0.25	0.89	1
Cathode 4.2 V aged	100	5.65	23.10	0.47	0.82	1
Cathode 4.0 V aged	100	6.08	37.07	0.61	0.84	1

Results from the rate capability test showed a decreased capacity at higher discharge rates and thus an increased resistance. As the 4.2 V-cell does not show significant increase in its aged state it is supposed that the cathode suffers from a diffusional limitation as well. To verify this assumption the diffusion properties of the cathode should be investigated.

We believe that the results for the charge-transfer process from the symmetric cells are representative to what is happening in the cell. Comparing the fitting data from the symmetric cells with the 18650 cells in the aged state gives a different statement concerning anode's and cathode's charge-transfer process. There it can be clearly seen that the change in the electrode's potential alters the reality.

4. Conclusions

In this study the effect of elevated temperature on a battery's lifetime has been investigated. Calendar aging was conducted on a commercial lithium ion battery containing $LiMn_2O_4$/$Li(Ni_{0.5}Co_{0.2}Mn_{0.3})O_2$ as cathode and graphite as anode material. Storage voltage was either 4.2 V or 4.0 V. It became evident, that calendar aging is predominantly driven by the storage voltage applied, if the cell is exposed to elevated temperatures. Already a reduction of 200 mV, i.e. from 4.2 V to 4.0 V has a positive impact on the cell's lifetime. The aging mechanisms in both cells can be roughly distinguished into capacity decrease during storage and increase of impedance/inner resistance.

The capacity fade is caused by:

1. Loss of cycleable lithium:

Due to massive consumption of cycleable lithium in the 4.2 V-cell for SEI layer growth the capacity decreases, which could be particularly seen in the potential curve of Figs. 11 and 12 and the SEM images in Fig. 13. Loss of cycleable lithium is also detected for the 4.0 V-cell, but at a much smaller extent. The reason for the difference is the amount of transition metal dissolution, which highly influences the growth of the SEI layer.

2. Loss of active material:

Small losses of active material at the cathode are assumed to have a contribution to the total capacity fade of the 18650 cell. The 4.2 V-cathode exhibits slightly higher losses of $LiMn_2O_4$ and $Li(Ni_{0.5}Co_{0.2}Mn_{0.3})O_2$ than the 4.0 V-cathode, which could be clearly shown in Table 1 and Fig. 10.

Reduced peak heights in the cyclic voltammetry indicate losses of both components of the active blend material. The loss of active material at the cathode could be either explained by isolated particles (cracked spinel particles and loosened NMC particles) or by transition metal dissolution from the positive active material.

The increase of the impedance/inner resistance is caused by:

1. Electrolyte decomposition:

Elevated temperatures and high storage potentials initiate the decomposition of the electrolyte's components like $LiPF_6$ as shown in Equation (3). The increase of the ohmic resistance in Figs. 4 and 5 clearly reveals that the electrolyte decomposition is higher for the 4.2 V-cell. This effect is probably not only caused by electrolyte decomposition and may be caused by a porous surface layer which is permeable for the electrolyte but acts as a hindering layer.

2. Variation of cathode impedance:

The impedance spectra of the aged symmetrical cathodes exhibit an ambivalent trend. The 4.2 V-cathode shows an equal charge-transfer resistance, while the 4.0 V-cathode exhibits a remarkable increase of its R_{ct}.

3. Diffusional limitation:

Comparing results from the rate capability test (decreased capacity) with results from impedance spectroscopy (reduced charge-transfer resistance) reveals that there should be a diffusional limitation inside the anode and cathode.

References

[1] J. Belt, V. Utgikar, I. Bloom, J. Power Sources 196 (2011) 10213–10221.
[2] M. Winter, J.O. Besehard, M.E. Spahr, P. Novák, Adv. Mater. 10 (1998) 725–763.
[3] P. Arora, R.E. White, M. Doyle, J. Electrochem. Soc. 145 (1998) 3647–3667.
[4] M. Wohlfahrt-Mehrens, C. Vogler, J. Garche, J. Power Sources 127 (2004) 58–64.
[5] M. Broussely, Ph. Biensan, F. Bonhomme, Ph. Blanchard, S. Herreyre, K. Nechev, R.J. Staniewicz, J. Power Sources 146 (2005) 90–96.
[6] EL-Cell GmbH, www.el-cell.com.
[7] C.H. Chen, J. Liu, K. Amine, J. Power Sources 96 (2001) 321–328.
[8] H. Schichlein, A.C. Müller, M. Voigts, A. Krügel, E. Ivers-Tiffée, J. Appl. Electrochem. 32 (2002) 875–882.
[9] A. Leonide, V. Sonn, A. Weber, E. Ivers-Tiffée, J. Electrochem. Soc. 155 (2008) B36–B41.
[10] V. Sonn, A. Leonide, E. Ivers-Tiffée, J. Electrochem. Soc. 155 (2008) B675–B679.
[11] J.P. Schmidt, T. Chrobak, M. Ender, J. Illig, D. Klotz, E. Ivers-Tiffée, J. Power Sources 196 (2011) 5342–5348.
[12] J. Illig, M. Ender, T. Chrobak, J.P. Schmidt, D. Klotz, E. Ivers-Tiffée, J. Electrochem. Soc. 159 (2012) A952–A960.
[13] B. Stiaszny, J.C. Ziegler, E.E. Krauß, J.P. Schmidt, E. Ivers-Tiffée, J. Power Sources 251 (2014) 439–450.
[14] T. Kawamura, S. Okada, J.-I. Yamaki, J. Power Sources 156 (2006) 547–554.
[15] T. Zheng, A.S. Gozdz, G.A. Amatucci, J. Electrochem. Soc. 146 (1999) 4014–4018.
[16] J. Vetter, P. Novák, M.R. Wagner, C. Veit, K.-C. Möller, J.O. Besenhard, M. Winter, M. Wohlfahrt-Mehrens, C. Vogler, A. Hammouche, J. Power Sources 147 (2005) 269–281.
[17] K.-W. Nam, W.-S. Yoon, H. Shin, K.Y. Chung, S. Choi, X.-Q. Yang, J. Power Sources 192 (2009) 652–659.
[18] Y. Liu, X. Li, H. Guo, Z. Wang, Q. Hu, W. Peng, Y. Yang, J. Power Sources 189 (2009) 721–725.
[19] P. Ramadass, A. Durairajan, B. Haran, R. White, B. Popov, J. Electrochem. Soc. 149 (2002) A54–A60.
[20] J. Bisquert, G. Garcia-Belmonte, F. Fabregat-Santiago, A. Compte, Electrochem. Commun. 1 (1999) 429–435.